THE WISCONSIN DYNAMICAL/MICROPHYSICAL MODEL (WISCDYMM) AND THE USE OF IT TO INTERPRET SATELLITE OBSERVED STORM DYNAMICS

Pao K. Wang
Department of Atmospheric and Oceanic Sciences
University of Wisconsin-Madison
1225 W. Dayton Street
Madison, WI 53706
U.S.A.

1 BRIEF DESCRIPTION OF THE CLOUD MODEL WISCDYMM AS CURRENTLY CONFIGURED

This paper will briefly report on the cloud model that has been used in our group for various researches but especially those related with the physics and dynamics atop thunderstorms. The successful applications of this model to investigate several satellite observed dynamical processes atop thunderstorms will also be summarized. The model is WISCDYMM (the Wisconsin Dynamic and Microphysical Model), developed in the author's research group. The earliest form was described in Straka (1989) and subsequently modified by others (Johnson et al. 1993, 1994; Lin and Wang, 1997; Wang, 2003). Its properties are described in the following subsections.

1.1 Grid Configuration and Time Step

WISCDYMM uses a uniform staggered grid in all directions, placing the wind components on the normal grid cell faces and the remaining variables at the grid cell centers (Arakawa-C grid). Typically, these cells are assigned equal dimensions in both horizontal directions while it is usually smaller in the vertical. The time step size, assumed uniform, is dictated by quasi-compressible computational stability requirements. The computational domain and resolution can be changed according to the needs of specific purposes. A typical setup of the grid for studying severe storm dynamics is given in the following: the grid mesh is 1.0 km horizontally and 0.5 km

vertically, with corresponding dimensions of 55 and 20 km for the model domain, while the time step is 3 s. In some cases, the resolution remains the same but the horizontal domain is expanded to 120 km × 100 km and the top boundary is set a 30 km. For the purpose of studying the water vapor transport across the tropopause (Wang, 2003), the vertical resolution was set at 200 m. The model also has been run with horizontal resolution of 500 m and good results were obtained.

1.2 Initialization

The initial fields in WISCDYMM simulations consist of two components: (a) a horizontally homogeneous base state closely adapted from a pre-storm rawinsounding, with no condensate and specifying the surface pressure from the sounding data, and (b) an impulse to initiate the modeled storm. The rawinsounding data, which have irregular vertical spacing, are linearly interpolated (without smoothing) to the appropriate model grid levels as potential temperature, either water vapor mixing ratio or relative humidity, and the horizontal wind components relative to the earth. Base-state pressure values above ground are derived from the surface pressure by assuming a hydrostatically balanced environment. So far, the initial impulse has been an ellipsoidal warm bubble in the lower central part of the model domain, with the same relative humidities as in the base state.

1.3 Model Physics

WISCDYMM predicts the three wind components, turbulent kinetic energy, potential temperature, pressure deviation and mixing ratios for water vapor, cloud water, cloud ice, rain, graupel/hail and snow. The model adapts the quasi-compressible, non-hydrostatic primitive equation system of Anderson et al. (1985), rearranging the mass continuity equation to predict the pressure deviation much as in the fully compressible 3D cloud model of Klemp and Wilhelmson (1978), but allows time steps ~3 times larger by assigning acoustic waves a reduced pseudo-sound speed roughly twice the maximum anticipated wind speed. As in Klemp and Wilhelmson, subgrid transports are parameterized via 1.5-order "K-theory" to predict turbulent kinetic energy, from which a time-and space-dependent eddy coefficient is diagnosed for momentum and set 35% larger for the heat and moisture predictands (Straka, 1989).

As elaborated by Straka (1989), a version of WISCDYMM called HPM (Hail Parameterization Model) features a bulk microphysics parameterization that entails water vapor and five hydrometeor types: cloud water, cloud ice, rain, graupel/hail and snow, with 37 individual transfer rates

(source/sink terms). Adapted largely from Lin et al. (1983) and Cotton et al. (1982, 1986), this package treats all hydrometeors as spheres except for cloud ice, which is treated as small hexagonal plates. Cloud water and cloud ice are assumed monodisperse, with zero fallspeed relative to the air. All three precipitation classes have inverse-exponential size distributions, with temperature-dependent intercepts for snow and graupel/hail, while the intraspectral variation of particle fallspeed versus diameter for each is assumed to satisfy a power law.

If necessary, WISCDYMM can also be run in the HCM (Hail Category Model) mode in which the evolution of hailstones can be tracked by studying the growth of hail sizes in a number (e.g., 25) of size bins. The HCM has been tested successfully in Straka (1989).

WISCDYMM is also programmed to activate one or more of the following three iterative microphysical adjustments (Straka, 1989) where and if needed:

- A saturation adjustment is performed to: (a) condense cloud water (or depose cloud ice) to eliminate supersaturation, releasing latent heat of evaporation (or sublimation), or (b) evaporate cloud water (or sublimate cloud ice) in subsaturated air until either saturation is reached or the cloud water (or cloud ice) is exhausted, absorbing latent heat instead. Cloud water is adjusted first and cloud ice second, incrementing the water vapor and temperature to suit. In-cloud saturation mixing ratios are weighted between their values with respect to (w.r.t.) water and ice in proportion to the relative amounts of cloud water and cloud ice respectively. Where no cloud is present, saturation is taken w.r.t. water or ice if the temperature is above or below 0C respectively. More than three iterations are rarely needed.

- Prior to the saturation adjustment, any cloud ice at temperatures above 0C is melted, and any cloud water at temperatures below -40C is frozen, respectively absorbing or releasing latent heat of fusion.

- After partial update of the moisture fields by advection and turbulent mixing, the decrement in each hydrometeor field due to the net sink (the sum of the individual microphysical sink terms) is compared to its available supply, defined as its partially updated mixing ratio plus the increment due to its net source (the sum of the individual microphysical source terms). If the net sink of a hydrometeor class exceeds its available supply, it is prorated downward along with each of its components so as to not exceed 25% of the available supply. The procedure is iterative because prorating down the sinks of one

class also reduces the corresponding source terms for one or more other classes, but more than two iterations are rarely needed.

1.4 Boundary Conditions

The lateral boundary conditions are similar to those in Klemp and Wilhelmson (1978). Reflection of outward-propagating gravity waves is suppressed by "radiation" conditions which advect each horizontal normal wind component out with a velocity equal to itself plus a prescribed constant outward gravity wave propagation of speed c*, except assigning zero advection in inflow of speed greater than c*. The other predictands at lateral boundary outflow locations are advected by upstream differencing.

Both the upper and lower boundaries are rigid lids. Variables at the top are held undisturbed, while reflection of upward-propagating gravity waves off the lid is suppressed by imposing an upper-level Rayleigh damping layer that abuts it. The lower boundary has four options: free-slip with no surface heat flux; semi-slip with no surface energy budget; no-slip with heat flux and no surface energy budget; or no-slip with heat flux, insolation and surface energy budget.

1.5 Interior Numerics

The current version of WISCDYMM uses forward time differencing and sixth-order flux-conservative Crowley spatial differencing (Tremback et al., 1987). To suppress nonlinear instability, a fourth-order numerical diffusion operator with a constant coefficient, as in Klemp and Wilhelmson (1978), is added in the discretized predictive equations at each time step.

2 SIMULATION OF THE 2 AUGUST 1981 CCOPE SUPERCELL THUNDERSTORM

Up to the present, WISCDYMM has been used primarily for simulating deep convective events. It has successfully simulates many cases of severe thunderstorms occurring in US and other parts of the world. To illustrate the capability of this model, the simulation results of the 2 August 1981 supercell storm occurred in Montana in the Midwest of US will be briefly presented. In later sections, the simulation results of this storm will be used as examples for understanding some thunderstorm dynamical processes as observed by meteorological satellites.

2.1 A Brief Description of the 2 Aug 1981 CCOPE Supercell

The storm chosen for the simulation for illustrating the plume-formation mechanism is a supercell that passed through the center of the Cooperative Convective Precipitation Experiment (CCOPE) (Knight, 1982) observational network in southeastern Montana on 2 August 1981. The storm and its environment were intensively observed for more than 5 h by a combination of seven Doppler radars, seven research aircraft, six rawinsonde stations and 123 surface recording stations as it moved east-southeastward across the CCOPE network. Miller et al. (1988) and Wade (1982) provided many of the observations in this section, especially those on the history of the storm. This case was chosen because it is a typical deep convective storm in the US High Plains and it provides much detailed observational data for comparison with model results with regard to dynamics and cloud physics, and the author's group has obtained successful simulations of it previously (Johnson et al., 1993, 1994).

2.1.1 Environmental Conditions

The initial conditions for the simulation are based on a 1746 MDT (Mountain Daylight Time) sounding (Fig.1) taken at Knowlton, Montana, approximately 90 km ahead of the storm. This sounding provided the most representative temperature and moisture profile available, with a massive convective available potential energy (CAPE) 3312 J kg^{-1} distributed over a comparatively shallow layer from the level of free convection LFC = 685 mb to the equilibrium level EL = 195 mb. The subcloud layer (below 730 mb) was nearly dry-adiabatic and well mixed, with a potential temperature close to 311.5 K, and also relatively moist because a surface low in north central Wyoming advected water vapor mixing ratios of 12-13 g kg^{-1} into the region on easterly winds. Above the subcloud region, a strong capping dry layer existed at approximately 710 mb, caused by warmer and drier air that had unexpectedly moved into the region after 1300 MDT. Wade (1982) gives some possible causes of this warming. The dry layer was significant in that it allowed the low-level air mass to continue warming for the remainder of the afternoon and become even more potentially unstable. From the dry layer to 450 mb, the environmental lapse rate was nearly dry adiabatic. The calculated indices from the Knowlton sounding (Total Totals index = 60, Lifted index = –9.4, and a K index =38) indicated that the air mass over eastern Montana on 2 August was very unstable, and hence very favorable for the development of deep convection.

Large vertical wind shear between lower and midlevels was also conductive to severe weather development. The 1746 MDT Knowlton

hodograph (not shown) indicated strong subcloud flow, veering nearly 70° from the surface layer to cloud base at 1.6 km AGL. The magnitude of the mean shear over the lowest 6 km was 0.008 s^{-1}. There was little directional shear above the cloud base, but vertical speed shears between the cloud base and 9 km were 0.006 s^{-1} (Miller et al., 1988). Taking into account the vertical wind shear and buoyancy effects, the Bulk Richardson Number for the pre-storm environment was 25, in the expected range for supercell storms. Some previous studies have pointed out that clockwise curvature of the wind shear vector over the lowest 2 km of the hodograph also favored development of the right-moving supercell.

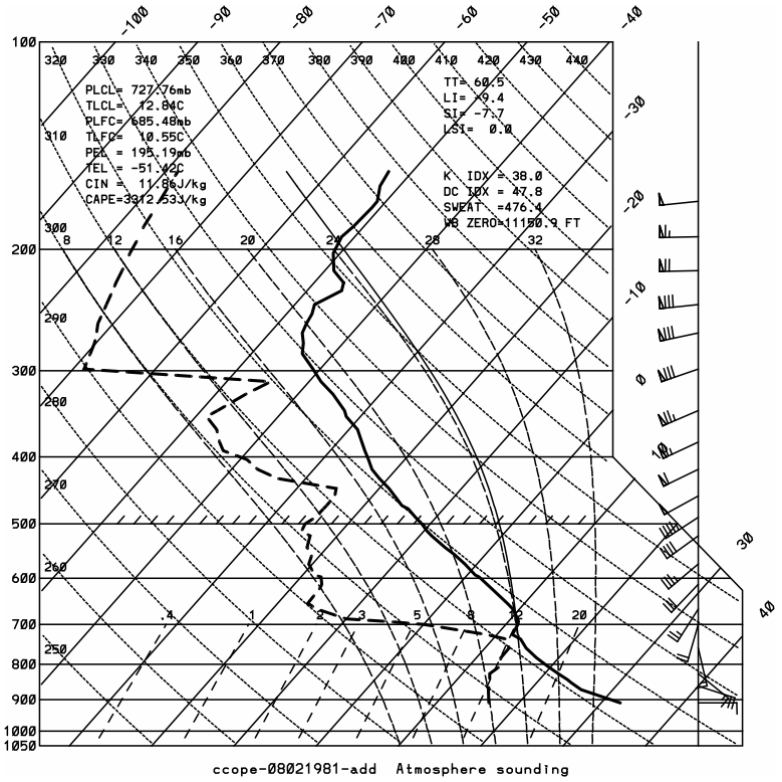

Fig. 1. The 1746 MDT Knowlton, Montana sounding on 2 August 1981. The solid curve is for temperature and dashed curve for dew point. The portion of dew point curve above 300 hPa, which was missing in the original sounding, is constructed using an average August 1999 HALOE water vapor profile over 40-60N.

2.1.2 Examples of Simulated Microphysical and Dynamical Fields

To illustrate the model performance, Figures 2 and 3 show the simulated hydrometeor mixing ratio and vertical velocity fields in the central east-west vertical cross-section of the storm at t = 40 min. In general the model results agree with the observed behavior of the supercell very well.

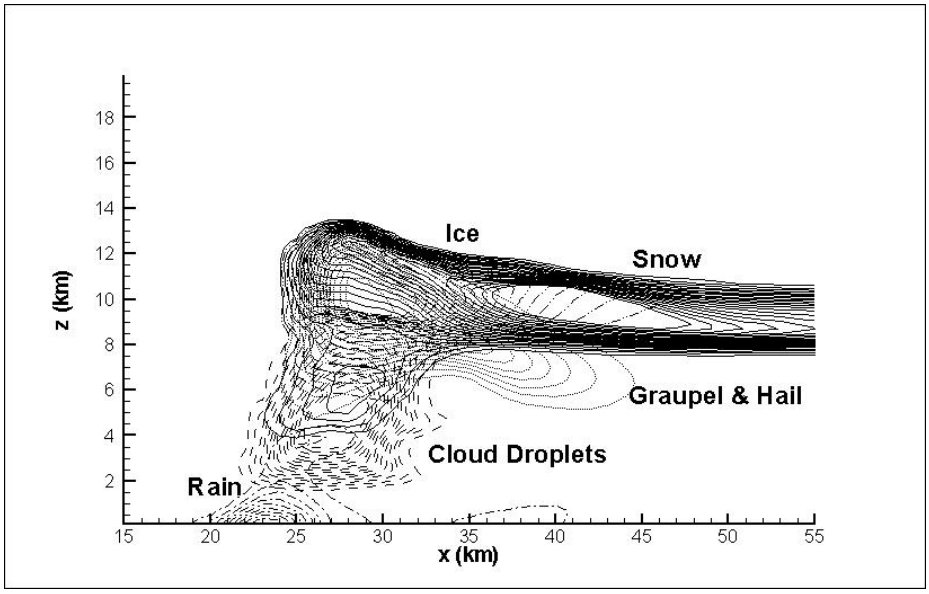

Fig. 2. Simulated hydrometeor mixing ratios and storm-relative vector wind projection field for the CCOPE storm of 2 August 1981, in X-Z (East-West) vertical cross-sections through the maximum updraft as of 90 min. Solid—snow, dotted—graupel & hail, dashed—cloud droplets, dash dot—rain, dash dot dot – cloud ice.

2.1.3 Simulation of Anvil Top Cirrus Plumes

As indicated before, WISCDYMM has been used successfully to study cloud dynamical and physical processes atop deep convective storms. One recent example is the identification of the physical mechanism that produces the cirrus plumes above the anvils of some severe thunderstorms.

Such plumes have been observed from satellite visible and infrared images and some details of them have been studied by a number of investigators (Setvak and Doswell, 1991; Levizzani and Setvak, 1996). Fig. 4 shows an example of such plumes. Since the anvils of these severe storms were already at the tropopause level, the plumes must have been higher up in the stratosphere. In one case, Levizzani and Setvak estimated that the plume was located at ~ 15 km which was about 3 km above the local tropopause at

the time. Since water vapor in the stratosphere has significant implications on the global climate process because of its strong absorption of infrared

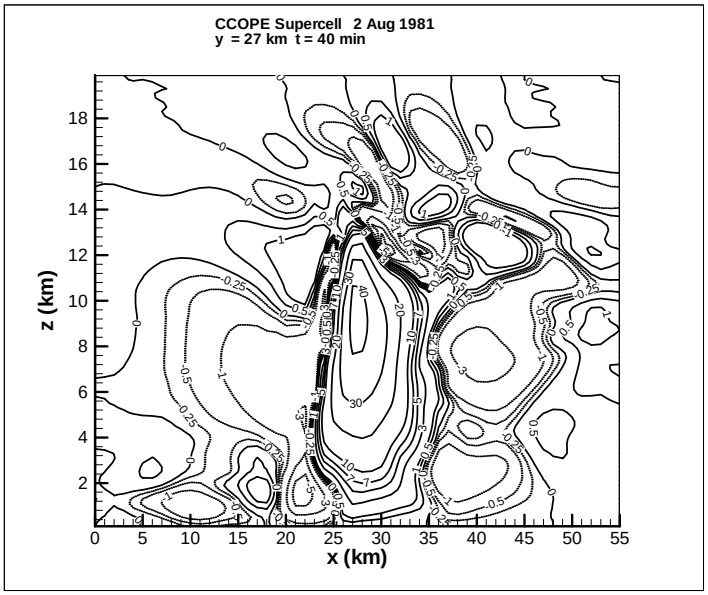

Fig. 3. The vertical velocity (w) field in the central east-west cross-section of the simulated storm at t = 40 min. Solid (dashed) contours represent positive (negative) w (in m s^{-1}).

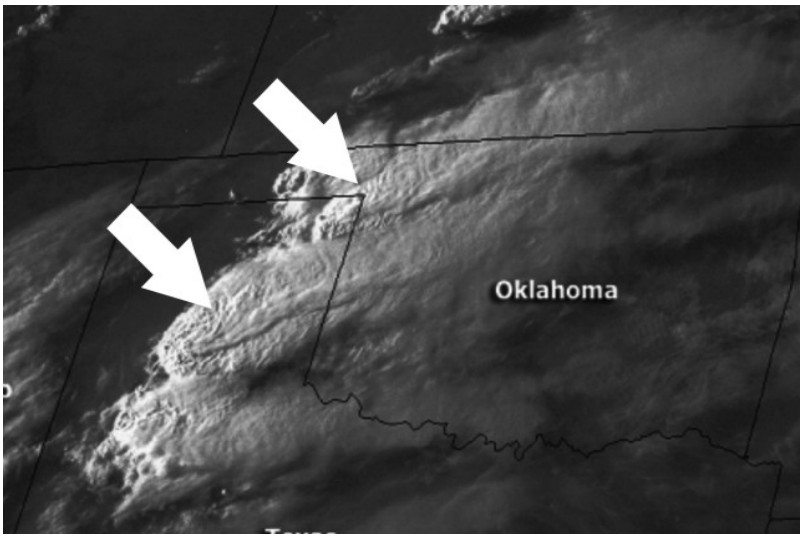

Fig. 4. GOES-8 composite image (cannel 1 + channel 3 + channel 4) on 6 May 2002 00:15 UTC showing plumes on top of thunderstorms (indicated by white arrows) in Texas and Oklahoma border region.(Courtesy of NOAA)

radiation, it is important to understand where the water vapor source is and how much is injected into the stratosphere.

In order to identify the physical mechanism responsible for the plume formation and the source of its water vapor, we studied the simulation results of the CCOPE supercell to see whether or not the simulated storm produces the same plume phenomenon. The answer turned out to be positive. Figs. 5 and 6 show the simulated plume phenomenon in the central cross-section view and 3D cloud top view respectively (Wang, 2003). The model-produced plumes exhibit nearly the same major characteristics of the observed ones, hence it is highly likely that the observed plumes must have been produced in a manner similar to that occurred in the simulated storm. Careful analysis of the model results indicate that the moisture forming the plumes come from the storm below, and the mechanism that eject moisture from the troposphere into the stratosphere is the breaking of cloud top gravity waves (Wang, 2003). This demonstrates that the results generated by the cloud model are realistic can be used as a substitute (when appropriate) for studying physical processes in thunderstorms whereas in-situ or remote observations are either difficult or can provide only limited temporal and spatial coverage.

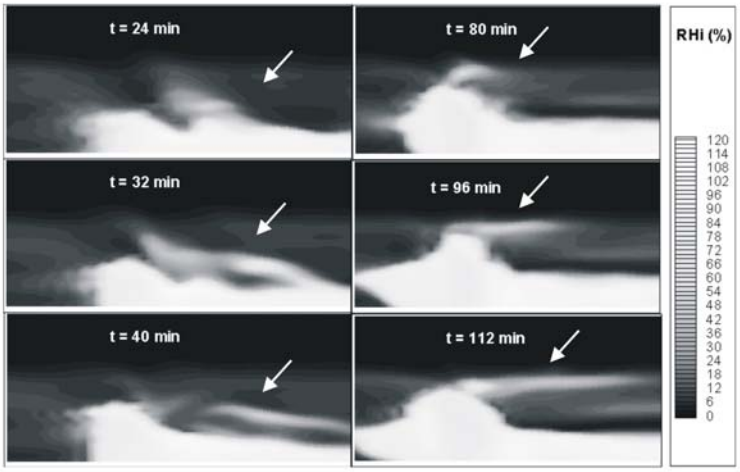

Fig. 5. Snapshots of modeled RHi (relative humidity with respect to ice) profiles at t = 24, 32, 40, 80, 96 and 112 min in the central east-west cross-section (y = 27 km), showing the plume feature above the anvil. Only the portion near the cloud top is shown. The vertical axis range is 10-20 km and horizontal axis range 20-55 km. (from Wang, 2003)

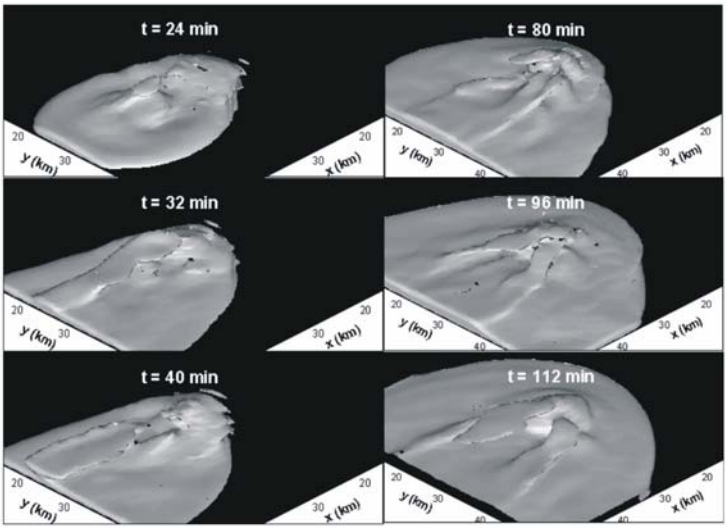

Fig. 6. Snapshots of 3D renderings for the 30% RHi contour surface at t = 24, 32, 40, 80, 96 and 112 min, showing the plume features above the anvil. Data below 10 km are windowed out. (from Wang, 2003).

2.1.4 Simulation of Fujita's Jumping Cirrus

Fujita (1982) described the observation of the jumping cirrus phenomenon above a thundercloud from an aircraft as follows:

> *"One of the most striking features seen repeatedly above the anvil top is the formation of cirrus cloud which jumps upward from behind the overshooting dome as it collapses violently into the anvil cloud".*

In a later paper he made a more elaborated report on this phenomenon (Fujita, 1989). Again due to the limited temporal and spatial coverage that can be provided by such observations, it is generally difficult to obtain detailed data for conclusively interpreting this phenomenon. At the time there were questions about whether it is possible to have cirrus clouds jumping upstream (i.e., against the wind). But by carefully studying the cloud top dynamics using the same WISCDYMM simulated results of the CCOPE supercell, it can be seen that the gravity wave breaking related to the anvil top plume phenomenon is also responsible for the jumping cirrus phenomenon. And the cirrus is not really jumping against the wind but it moves upstream only relative to the storm. If we keep in mind that the simulated storm is moving at ~ 30 m/sec during its development, then the cirrus is still moving downwind relative to the surface. Fig. 7 shows a series of the rendered cloud top humidity profiles that illustrate this process.

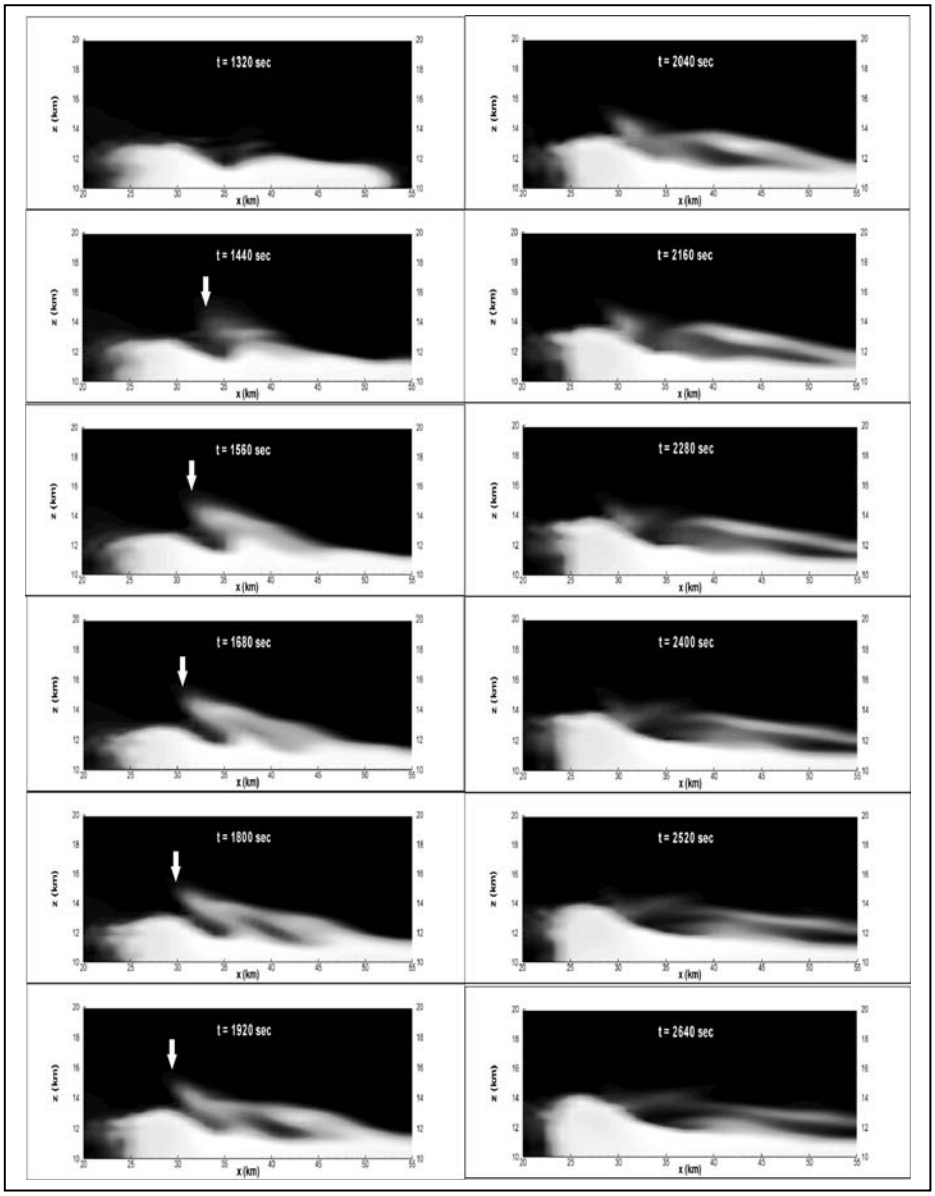

Fig. 7 Snapshots of the RHi profiles in the central east-west cross-section of the simulated storm from t = 1320 s to 2640 s. The RHi scale is similar to that in Fig. 5.

Acknowledgments. This work is partially supported by NSF Grants ATM-0234744 and ATM-0244505 to the University of Wisconsin-Madison.

References

Anderson, J. R., K. K. Droegemeier and R. B. Wilhelmson, 1985: Simulation of the thunderstorm subcloud environment. *Preprints, 14th Conf. On Severe Local Storms.* Indianapolis, IN., *Amer. Meteor. Soc*., 147-150.

Cotton, W. R., M. A. Stephens, T. Nehrkorn, and G. J. Tripoli, 1982: The Colorado state University three-dimensional cloud model - 1982. Part II: An ice phase parameterization. *J. Rech. Atmos*., 16, 295-320.

Cotton, W. R., Tripoli, G. J., R. M. and Mulvihill, E.A., 1986: Numerical simulation of the effects of varying ice crystal nucleation rates and aggregation processes on orographic snowfall. *J. Clim. Appl. Meteorol.*, 25, 1658-1680.

Fujita, T. T., 1982: Principle of stereographic height computations and their application to stratospheric cirrus over severe thunderstorms, *J. Meteor. Soc. Japan*., *60*, 355-368.

Fujita, T. T., 1989: The Teton-Yellowstone tornado of 21 July 1987. *Mon. Wea. Rev*., *117*, 1913-1940.

Johnson, D. E., and P. K. Wang, and J. M. Straka, 1994: A study of microphysical processes in the 2 August 1981 CCOPE supercell storm. *Atmos. Res.* 33, 93-123.

Klemp, J. B., and R. B. Wilhelmson, 1978: The simulation of three-dimensional convective storm dynamics. *J. Atmos. Sci*., 35, 1070-1096.

Knight, C. A., Ed., 1982: The Cooperative Convective Precipitation Experiment (CCOPE), 18 May-7 August 1981. *Bull. Amer. Meteor. Soc*., 63, 386-398.

Lin, Hsin-Mu, and Pao K. Wang, 1997: A numerical study of microphysical processes in the 21 June 1991 Northern Taiwan mesoscale precipitation system. *Terres. Atmos. Oceanic Sci*., ., 8, 385-404.

Lin, Y. L., R. D. Farley, and H. D. Orville, 1983: Bulk parameterization of the snow field in a cloud model. *J. Climate Appl. Meteor*., 22, 1065-1092.

Miller, L. J., D. Tuttle, and C. A. Knight, 1988: Airflow and hail growth in a severe northern High Palins supercell. *J. Atmos. Sci*., *45*, 736-762.

Wade, C. G., 1982: A preliminary study of an intense thunderstorm which move across the CCOPE research network in southeastern Montana. *Proc. Ninth Conf. On Weather Forecasting and Analysis*. Seattle, WA, Amer. Meteor. Soc., 388-395.

Setvak, M., Rabin, R. M., Doswell III, C. A., and Vincenzo Levizzani, 2002: Satellite observations of convective storm tops in the 1.6, 3.7 and 3.9 mm spectral bands. *Atmos. Res*., *67-68*, 607-627.

Levizzani, V., and M. Setvak, 1996: Multispectral, high resolution satellite observations of plumes on top of convective storms. *J. Atmos. Sci*., 53, 361-369.

Straka, J. M., 1989: Hail growth in a highly glaciated central High Plains multi-cellular hailstorm. Ph.D. Diss., Dept. Meteorology, Universitiy of Wisconsin, Madison, 413 pp.

Tremback, C. J. Powell, W. R. Cotton, and R. A. Pielke, 1987: The forward-in-time upstream advection scheme: Extension to higher order. *Mon, Wea. Rev., 115*, 540-555.

Wang, P. K., et al., 2001: A cloud model interpretation of the enhanced V and other signatures atop severe thunderstorms. *Preprint. 11th Conference on Satellite Meteorology and Oceanography*, 15-18 Oct 2001, Madison, American Meteorological Society. 402-403.

Wang, P. K., 2003: Moisture Plumes above Thunderstorm Anvils and Their Contributions to Cross Tropopause Transport of Water Vapor in Midlatitudes. *J. Geophys. Res., 108(D6*), 4194, doi: 10.1029/2003JD002581